



Systematic study of the interdependence of exposure and development conditions and kinetic modelling for optimizing low-energy electron beam nanolithography

M.A. Mohammad^a, T. Fito^{a,b}, J. Chen^b, S. Buswell^c, M. Aktary^c, M. Stepanova^{a,b,*}, S.K. Dew^a

^a Department of Electrical and Computer Engineering, University of Alberta, Edmonton, Canada T6G 2V4

^b National Institute for Nanotechnology NRC, Edmonton, Alberta, Canada T6G 2M9

^c Applied Nanotools Inc., Edmonton, Alberta, Canada T6E 5B6

ARTICLE INFO

Article history:

Received 12 September 2009

Accepted 10 November 2009

Available online 14 November 2009

Keywords:

Nanofabrication

EBL

Low-voltage exposures

Kinetics of resist development

Kinetic modelling

ABSTRACT

In this work, we outline our extensive study of nanostructures with 15–35 nm lateral dimensions fabricated in PMMA employing 3–30 keV electrons. We have analysed the impact of the exposure voltage and dose, as well as development time and temperature, on the 3D morphology and quality of the nanoscale gratings in PMMA. We demonstrate that, in addition to the exposure conditions that are routinely optimized in standard EBL techniques, post-exposure resist processing is also a crucial factor and should be co-optimized when fabricating dense nanopatterns in the moderate to low voltage regimes. We analyze the potential of employing low-voltage exposures combined with cold development, and discuss factors affecting resolution and sensitivity of EBL at the nanoscale.

© 2009 Elsevier B.V. All rights reserved.

1. Introduction

As requirements for electron beam lithography (EBL) have progressed toward the sub-25 nm regimes, major challenges have emerged of introducing controllable radiation-induced changes at molecular-size scales, within a reasonable tradeoff with the applicability of the standard materials, as well as cost and simplicity of the processes. Due to the proximity effect, this becomes particularly demanding when dense patterns with closely positioned features must be fabricated. Achieving deep nanoscale resolutions in high density patterns at industrially-relevant throughputs requires new approaches to resist design, exposure strategies, and development techniques. Within the last decade, numerous research groups have invested a significant effort to explore the resolution limits of deep nanoscale EBL. In particular, optimizing the development conditions such as the developer formula [1–3] and development temperature [2,4,5] have been found effective to achieve improvements in resolution at the ~20 nm dimensions. However, the interplay of molecular mechanisms involved in both the electron–resist interaction and in the polymer dissolution (development) stages of nanolithography is still inadequately understood.

Furthermore, most of the research employed relatively high exposure voltages of at least 30 keV or higher. Low-voltage exposures were significantly less frequent, mostly because of the limitations in resolution of stronger forward scattering. At the same time, voltages at or below the 10 keV regimes have the advantage of requiring lower doses [6]. Moreover, ultra low voltage electrons in the 1–3 keV regimes deposit most of their energy within the resist decreasing dramatically the proximity effect [6,7]. Strong forward scattering of low-energy electrons, which is routinely believed to be the major resolution-limiting factor, may alternatively be employed to create nanoscale three-dimensional profiles in the resist [8]. Realizing this potential, however, requires a thorough understanding of the intricate interplay of the numerous EBL process control parameters including exposure, development, and other post-exposure steps.

In this article, we outline our study, both experimentally and theoretically, of the impact of the major EBL process factors on the quality and process sensitivity when fabricating dense nanoscale gratings in PMMA using low to medium (3–30 keV) exposure energies. We consider dense arrays of periodic lines (gratings) as a convenient benchmark nanostructure. Employing these grating patterns, we analyze typical morphological regimes, which we visualize by SEM. We interpret the conventional characteristics of the EBL process, such as resolution and sensitivity, in terms of the quality of the morphologies. By this we achieve morphology-bound interpretations of the sensitivity and resolution, which is

* Corresponding author. Address: Department of Electrical and Computer Engineering, University of Alberta, Edmonton, Canada T6G 2V4. Tel.: +1 780 641 1717. E-mail address: Maria.Stepanova@nrc-cnrc.gc.ca (M. Stepanova).

directly representative of the quality of the fabricated nano-patterns.

2. Experiment

The experimental methodology that we have employed has been described in detail elsewhere [9,10]. In brief, cleaned silicon substrates were spin coated with 950 k PMMA layers of thickness 47–55 nm. Sets of periodic grating patterns were generated (Raith 150). The exposed samples were developed in a 1:3 MIBK:IPA mixture followed by an IPA stopper rinse. We varied the developer temperature between $-15\text{ }^{\circ}\text{C}$ and $22\text{ }^{\circ}\text{C}$ using a cold plate, and employed development times from 5 s to 20 s. The stopper temperature was the same as that of the developer. We imaged the samples using a Hitachi S-4800 FE-SEM instrument. In addition to plan-view imaging of the grating morphologies, we also examined cross-sectional profiles. For this we fabricated long (up to 2 mm) grating patterns, which were manually cleaved while dipped in liquid nitrogen. Before SEM imaging, we coated our samples by sputtering (Kurt J. Lesker Co.) an approximately 6 nm thick chromium anti-charging layer.

Fig. 1 provides examples of the cross-sectional and plan-view images, and also summarizes the typical resist morphologies for gratings. In the low dose regime, the limiting factor is underexposure resulting in an insufficient resist clearance, whereas at increased doses, the patterns degrade through collapse, when the interline walls are bent or displaced [9].

Fig. 2a and b presents favorable dose windows as functions of the development time, at various developer temperatures, for gratings with 70 nm and 50 nm pitches, respectively. In the figures, the solid lines show the dose boundaries for underexposure and the dashed lines show the boundaries for collapse. The minimum applicable doses (denoted as d_{\min}) represent the sensitivity of the EBL process. It can be seen that decreased development temperatures require higher exposure doses, i.e. decrease the sensitivity. Thus, development of a 70 nm pitch grating at $-15\text{ }^{\circ}\text{C}$ requires an approximately 4 times higher line dose to obtain clearance than development at room temperature (RT). The regions between the solid and dashed lines in Fig. 2 represent the favorable dose windows where quality gratings may be fabricated. It can be seen that for a 70 nm pitch grating, decreasing the development temperature from RT to $-15\text{ }^{\circ}\text{C}$ results in an increase in the width of applicable line dose window, $d_{\max}-d_{\min}$, by an order of magnitude. In gratings with 50 nm pitch, the window $d_{\max}-d_{\min}$ approximately doubles when the development temperature changes from $-5\text{ }^{\circ}\text{C}$ to $-15\text{ }^{\circ}\text{C}$. The broader applicable process window at decreased development temperature allows for more control over properties of the fabricated pattern, such as the aspect ratio. Moreover, using the cold development allows lower feature dimensions to be

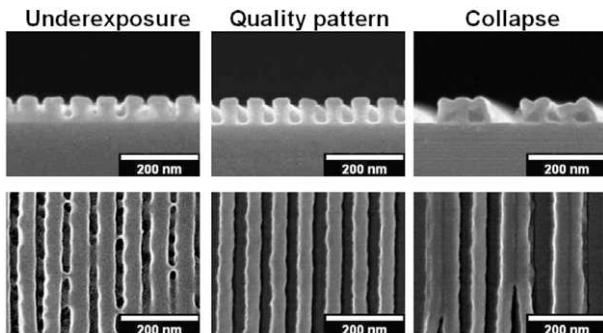


Fig. 1. Cross-sectional (top) and plan-view (bottom) SEM images for under-exposed (left), well-done (middle), and collapsed (right) gratings in PMMA on a Si substrate.

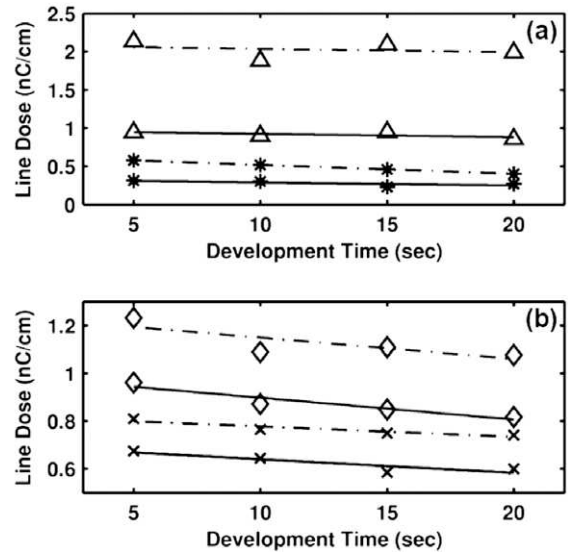


Fig. 2. The applicable dose windows for 70 nm pitch (a) and 50 nm pitch (b) gratings showing minimum (solid lines) and maximum (dashed lines) doses for quality patterning with 10 keV exposures. The symbols indicate: room temperature (stars), $-5\text{ }^{\circ}\text{C}$ (crosses), and $-15\text{ }^{\circ}\text{C}$ (triangles and diamonds) (adapted from Ref. [10]).

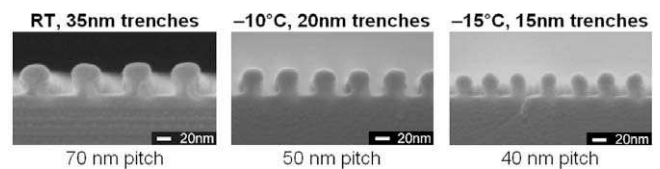


Fig. 3. Examples of optimized nanoscale patterns fabricated in PMMA with 10 keV exposure voltage for decreased development temperatures. The initial PMMA thickness was 55 nm for the 70 and 50 nm pitch, and 47 nm for 40 nm pitch.

achieved. As demonstrated in Fig. 3, using development temperatures of $-10\text{ }^{\circ}\text{C}$ and $-15\text{ }^{\circ}\text{C}$ allow fabrication of 50 nm and 40 nm pitch gratings with trenches of 20 nm and 15 nm in width, which could not be achieved by room temperature development with the given resist thicknesses.

To conclude, cold development results in a strong increase in the applicable dose window and improves the resolution. However, this is accompanied by a drop in the process sensitivity.

Next we explore the role of exposure energy on cross-sectional profiles for 70 nm pitch gratings fabricated at 3 keV, 10 keV, and 30 keV. The grating exposed with 3 keV shows pronounced undercuts because of strong forward scattering of electrons [7], whereas 30 keV exposures produce almost straight interline walls as shown in Fig. 4. Fig. 5 presents the applicable dose windows when the exposure voltages of 3 keV, 10 keV, and 30 keV are employed to fabricate a 70 nm pitch grating. It can be seen that increasing the electron energy from 3 keV to 30 keV results in a dramatic increase of the dose windows. However, the minimum applicable line doses also increase roughly in proportion to the electron energy, resulting in a significantly lower sensitivity for 30 keV voltages. In contrast, 3 keV exposures provide a better sensitivity. We have thoroughly studied the tradeoffs of resolution and sensitivity by varying the exposure energy (3–30 keV), development temperature ($-15\text{ }^{\circ}\text{C}$ –RT) and time (5–20 s) for 50 nm and 70 nm pitch gratings. We found that 3 keV voltage exposures combined with cold development at $-15\text{ }^{\circ}\text{C}$ still led to a strong improvement in the sensitivity. For both 70 nm and 50 nm pitches, the minimum applicable line dose d_{\min} was approximately half for the 3 keV, cold

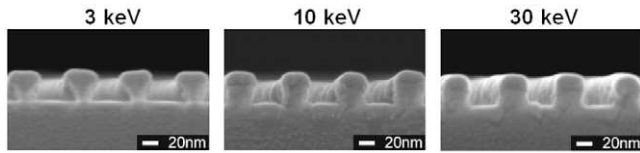


Fig. 4. PMMA gratings exposed using 3 keV, 10 keV, and 30 keV voltages.

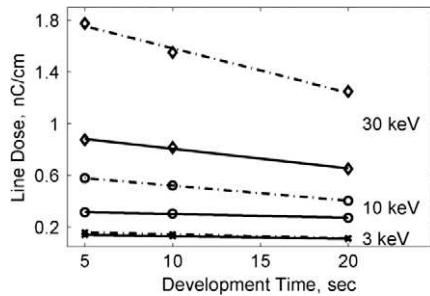


Fig. 5. Applicable dose windows for 70 nm pitch gratings using the exposure voltages of 3 keV, 10 keV, and 30 keV. The samples were developed at RT, and the initial PMMA thickness was 55 nm.

development processes than for the 30 keV, RT ones. Although the applicable dose window $d_{\max}-d_{\min}$ was 2–5 times narrower for 3 keV than for 30 keV, this was sufficient to fabricate 20 nm wide trenches. Thus, by combining 3 keV exposures with cold development, it is possible to profit through an improvement in sensitivity and yet obtain reasonably broad dose windows for nanoscale resolution. However, the conditions for exposure (energy, dose) and development (temperature, time) are intimately interrelated and should be selected carefully. In practice this may mean that 4 or even more process parameters must be co-optimized for a given resist–substrate–developer combination in order to reach ultimate resolution. To best understand the relevant trends and forecast the outcomes, appropriate numeric models should be employed and/or developed. In the next section, we outline some of numerical approaches that we found efficient for interpreting, systematising, and optimising nanoscale EBL.

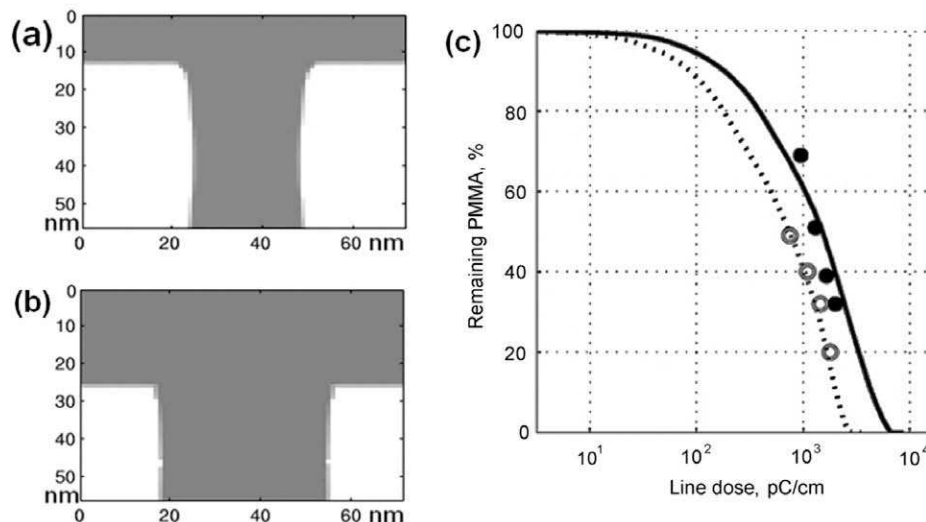


Fig. 6. (a, b) computed cross-sectional profiles (white – PMMA, grey – no PMMA) in a 70 nm pitch grating exposed by 10 keV electrons with the doses of 700 pC/cm and 1300 pC/cm, respectively, and developed at -10°C during 20 s; (c) computed (lines) and experimental (symbols) percentages of remaining PMMA as functions of the dose, in a 70 nm pitch grating developed at -15°C during 5 s (solid line and filled symbols) and 20 s (dotted line and open symbols).

3. Theory and finite-element modelling

To analyze kinetics of development of exposed PMMA, we firstly compute 3D distributions of the probability of polymer main-chain scission in the resist [11]. This differs from standard approaches that map energy deposition. Next, we convert the local probability of scission into the local volume fractions of PMMA fragments of various size $\varphi_n(x, y, z)$, where n is the number of monomers in a fragment, for which we employ the geometric distribution. The kinetic process of clearance is described by the movement of the resist–developer interface, which depends on the local distribution of fragments. We define the rate of dissolution by $v = dL/dt$, where L is the depth of shrinking of the resist. The kinetics of shrinking is described by [12]:

$$\frac{dL}{dt} = \eta D L^{-1}. \quad (1)$$

Here $D(x, y, z)$ is the local diffusivity of PMMA fragments and η is a constant coefficient that depends on the interaction of developer with PMMA. In the case of constant diffusivity D , Eq. (1) predicts the dependence $v \sim (D/t)^{1/2}$, where t is time of development. Elsewhere [12] we have demonstrated that Eq. (1) can be derived from the general mean-field theory of diffusion in polymeric systems [13]. The approximate model of resist shrinking described by Eq. (1) implies that at the nanoscale, the rate of resist dissolution is a function of the entire history of the process of development, and thus depends on time explicitly. This is different from most available models of EBL resist development, which assume the existence of a stationary regime with a constant rate of dissolution [14–16].

For the diffusivity of PMMA fragments of size n , we employ the proportionality $D_n \sim n^{-\alpha} \exp(-U/kT)$, where U is the activation energy and the factor $n^{-\alpha}$ describes the mobility of fragments of size n in a medium whose properties are represented by power α . In most polymers, α varies from 1 in dilute solutions of small molecules to 2 for denser melts of longer polymer chains [17,18]. In exposed PMMA, an effective location-dependent diffusivity can be introduced, $D'(x, y, z) = \langle \eta D_n \rangle = \langle \beta n^{-\alpha} \rangle$, where $\alpha = 1 + \langle n \rangle / \gamma$ for average fragment size $\langle n \rangle$ less than γ , and $\alpha = 2$ otherwise.

We have implemented an efficient finite-element numeric algorithm to model the process of development [12]. We execute a sequence of discrete dissolution steps, where time δt required to

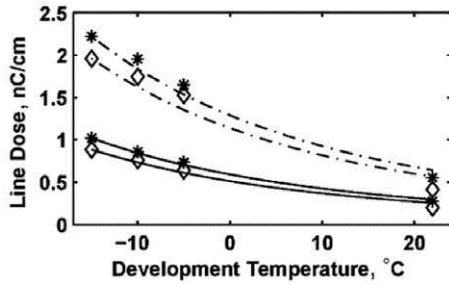


Fig. 7. Comparison of Eq. (2) for the boundary doses d_{\min} (solid lines) and d_{\max} (dashed lines) as functions of development temperature for a 70 nm pitch grating exposed with 10 keV electrons and developed during 5 s (upper curves) and 20 s (lower curves). The symbols indicate experiment for development times of 5 s (stars) and 20 s (diamonds) (adapted from Ref. [10]).

dissolve a resist layer of thickness δL is determined by $\delta t = 2L\delta L/D(x, y, z)$. The simulation provides the location of the 3D resist-developer interface as a function of time, with a 1 nm spatial resolution. The model parameters β and γ may depend on temperature but not on other process conditions, and are evaluated by fitting the computed percentages of PMMA left on the substrate to the corresponding experimental results. We obtain these from our SEM cross-sectional profiles for gratings.

Fig. 6 presents examples of our computed cross-sectional clearance profiles for a 70 nm pitch grating (a, b) and the amount of remaining PMMA (c). The latter is also compared with corresponding experiments. The kinetic model describes the broadening of the clearance trenches in gratings, the thinning of the walls, and the shrinkage of the thickness of the resist during development. Figs. 6a and b also demonstrate that at a given development time, the locations at which the resist clearance occurs depend on the exposure dose. At lower doses PMMA is removed preferentially from the intensely exposed trenches where fragments are the most mobile (Fig. 6a), whereas more intense exposures allow for partial dissolution of interline walls containing heavier, less mobile fragments (Fig. 6b).

One can conclude that dissolution of the exposed PMMA can be represented as a kinetic diffusion-like process, with the average effective diffusivity $D(x, y, z)$ determined by the local fragmentation of the resist. Thus, for moderate exposure doses, the mean size of fragments $\langle n \rangle$ is inversely proportional to the local probability of scissions [11], which in turn is related with exposure dose d , so that $\langle n \rangle \sim 1/d$. Assuming for simplicity that $D \sim \langle n \rangle^{-z} \exp(-U/kT)$ [17], one obtain the proportionality $D \sim d^z \exp(-U/kT)$. Adopting further that for a given development time and pattern geometry, the boundary applicable doses for quality nanofabrication, d_{\min} and d_{\max} , correspond to the same value of D in the exposed trenches and in the walls, respectively, we obtained the following equation for the temperature dependence of these doses d_{\min} and d_{\max} [10]:

$$d_{\min, \max} = d_{\min, \max}^{\text{ref}} \exp\left(\frac{U}{\alpha k} (1/T - 1/T^{\text{ref}})\right). \quad (2)$$

Here 'ref' indicates reference values for the doses d_{\min} and d_{\max} and for temperature. In Fig. 7, we compare Eq. (2) with the experimental

dependencies for $d_{\min}(T)$ and $d_{\max}(T)$ in a 70 nm pitch grating exposed with 10 keV electrons, using the experiments for -15°C as reference and employing the estimated value $U/\alpha = 0.22$ eV. It can be seen that Eq. (2) describes very well the broadening of the applicable dose window with the decrease of the development temperature. After the model, the minimum applicable dose window d_{\min} can be interpreted as the dose at which PMMA fragments in the intensely exposed trenches are mobile enough to be removed over the time of development. The maximum applicable dose d_{\max} is, in turn, determined by molecular diffusion processes occurring in the walls. Accordingly, the kinetics of molecular mobility in the various locations of the resist emerges as a major factor determining both the resolution and sensitivity of EBL at the nanoscale.

4. Summary

To satisfy the requirements for quality nanofabrication, at least four EBL process parameters (exposure voltage, dose, development temperature, and time) must be co-optimized for a given resist-substrate-developer combination. Our approach comprises a thorough experimental study complemented by numerical analysis that allows interpreting and systematising the observed trends. Based on this framework, we developed optimized processes combining low-voltage exposures with cold development, and elucidated the role of the kinetic factors in determining the sensitivity and resolution of nanoscale EBL.

Acknowledgements

The authors thank Marko van Daltsen for his assistance with the EBL process, and Zsolt Szabo for designing dose test samples and his programming contributions. The work was supported by NINT-NRC, NSERC, Alberta Ingenuity, iCORE, and Raith GmbH.

References

- [1] O. Dial, C.C. Cheng, A. Sherer, J. Vac. Sci. Technol. B 16 (1998) 3887.
- [2] M. Yan, S. Choi, K.R.V. Subramanian, I. Adesida, J. Vac. Sci. Technol. B 26 (2008) 2306.
- [3] S. Yasin, D.G. Hasko, H. Ahmed, Microelectron. Eng. 61–62 (2002) 745.
- [4] B. Cord, J. Lutkenhaus, K.K. Berggren, J. Vac. Sci. Technol. B 25 (2007) 2013.
- [5] L.E. Ocola, A. Stein, J. Vac. Sci. Technol. B 24 (2006) 3061.
- [6] K.-D. Schock, F.E. Prins, S. Strähle, D.P. Kern, J. Vac. Sci. Technol. B 15 (1997) 2323.
- [7] Y.H. Lee, R. Browning, N. Maluf, G. Owen, R.F.W. Pease, J. Vac. Sci. Technol. B 10 (1992) 3094.
- [8] W. Brünger, E.B. Kley, B. Schnabel, I. Stolberg, M. Zierbock, M. Plontke, Microelectron. Eng. 27 (1995) 135.
- [9] M.A. Mohammad, S.K. Dew, K. Westra, et al., J. Vac. Sci. Technol. B 25 (2007) 745.
- [10] M.A. Mohammad, T. Fito, J. Chen, M. Aktary, M. Stepanova, S.K. Dew, J. Vac. Sci. Technol. B. in press.
- [11] M. Aktary, M. Stepanova, S.K. Dew, J. Vac. Sci. Technol. B 24 (2006) 768.
- [12] T. Fito, M.A. Mohammad, Zs. Szabó, J. Chen, M. Aktary, S.K. Dew, M. Stepanova, in preparation.
- [13] S.M. Scheinhardt-Engels, F.A.M. Leermakers, G.J. Fleer, Phys. Rev. E. 68 (2003) 011802.
- [14] J.S. Greeneich, J. Vac. Sci. Technol. 12 (1974) 5264.
- [15] G. Han, M. Khan, F. Cerrina, J. Vac. Sci. Technol. B 21 (2003) 3166.
- [16] D.G. Hasko, S. Yasin, A. Mumtaz, J. Vac. Sci. Technol. B 18 (2000) 3441.
- [17] L. Masaro, X.X. Zhu, Prog. Polym. Sci. 24 (1999) 731.
- [18] B.A. Miller-Chou, J.L. Koenig, Prog. Polym. Sci. 28 (2003) 1223.